UNIVERSITÀ
DEGLI STUDI
DI PADOVA

UNIVERSITY OF PADUA

Department of Industrial Engineering

Master Thesis in Energy Engineering

Design and realization of the electronic control unit of a DCCT sensor for beam current measurement of the SPIDER experiment

Supervisor
Prof. Marconato Nicolò

Master Candidate
Samuele Bisinella

ID Student
2052440

Academic Year
2023 - 2024

Abstract

The SPIDER experiment (Source for Production of Ion of Deuterium Extracted from Rf plasma) is currently in shut-down for repairs, modifications, and improvements based on the experience gained in the first years of operation since 2018.

Among these upgrades, the installation of the "Beamlet Group Current Monitors" (BGCM) diagnostic is planned for measuring the beam current for each of the 16 beamlet groups in the acceleration grids.

Therefore, it is necessary to design a current sensor capable of measuring the beam current exiting the ground grid for each of the 16 beamlet aperture groups. The 16 signals from each sensor will provide the measurement of the total beam current, allowing, in addition, the assessment of its uniformity.

The main requirements for the current sensor are as follows:

- Measurement of both direct current (DC) and variable current (AC, tens of kHz);
- Operation in high vacuum (10^{-6} mbar);
- Resistance to significant thermal loads;
- High resolution and precision in a current range between 100 mA and 3 A;
- Immunity to external DC magnetic fields;
- Immunity to the 1 MHz radiofrequency component of the beam current;
- Immunity to electrical breakdowns;
- Mechanical compatibility with the available spaces in front of each beamlet group.

The technology of the so-called Direct Current Current Transformer (DCCT) is considered the most promising for this type of current sensor, in terms of sensitivity, robustness, and immunity to disturbances.

The proposed thesis is part of the necessary activities for developing a sensor using this technology for the specific case of SPIDER. The thesis activity involves determining the best electronic components suitable for realizing the

power supply and control system of the sensor and its subsequent implementation. A first research phase is planned to determine the best technologies, followed by an implementation phase.

Contents

1 Introduction

The greater awareness of environmental issues, driven by an escalation in the climate change problems, highlights the impossibility of continuing on the path of fossil fuels as an energy source. Global policies toward the decarbonization of the energy sector support research on both renewable sources (biomass, photovoltaic, wind turbines, etc.) and nuclear fusion. In a scenario where about 40% of global annual CO_2 emissions come from the electricity and heat sector, nuclear fusion represents a promising energy source that will allow the production of electricity on a large scale in a safe and eco-friendly way.

In detail, nuclear fusion utilizes the energy released during the fusion of two light nuclei. During this process, a fraction of the mass of the nuclei is converted to energy following the well-known Einstein equation:

$$E = mc^2 \tag{1}$$

For the reaction to occur, it requires that the energy possessed by the individual atoms is sufficient to overcome the electrostatic repulsion force between particles. For this reason, the entire reaction is performed within a high-temperature ionized gas called plasma. This plasma, in stars, is confined by gravitational forces, while on Earth, it can be confined by means of strong magnetic fields in suitable configurations.

The energy released by the fusion process between Tritium and Deuterium atoms, generates 3.3×10^{11}J/g, which corresponds to:

- 10^7 times the energy generated by the combustion of 1 g of coal;
- 4 times the energy generated by the nuclear fission of 1 g of ^{235}U.

1.1 ITER

ITER (International Thermonuclear Experimental Reactor) is an international project born with the purpose of proving the scientific and technological feasibility of nuclear fusion as a new energy source.

The project consists in the realization of an experimental nuclear fusion reactor in a Tokamak magnetic configuration, inside which the reaction between the two isotopes of hydrogen (Deuterium and Tritium) will take place. Among the possible nuclear fusion reactions, the one between D and T guarantees the highest cross-section at low temperature, making it more interesting. The reaction can be represented as follows:

$$T + D \rightarrow \alpha(3.5MeV) + n(14.1MeV) \tag{2}$$

The nuclei of the two isotopes fusing together produce:

- An α particle (helium nucleus), which, being confined within the plasma due to its natural charge, contributes, thanks to its high energy content, to achieve the ignition, that is the condition in which the heat produced by the nuclear reaction is sufficient to self-sustain the process;
- A neutron, which, being instead uncharged, can escape through the magnetic confinement of the plasma and be utilized to heat a suitable coolant for the generation of electric energy.

The generated thermal power (P_{th}) can thus be seen as the summation of two factors:

$$P_{\text{th}} = P_{\alpha} + P_{\text{n}} \tag{3}$$

Where:

- P_{α} is the power for heating the plasma through collisions (about 20% of P_{th})
- P_{n} is the power transferred to a suitable coolant for electricity generation (about 80% of P_{th})

Considering that only a fraction of the total energy is used to heat up the plasma, an external heating power (P_H) is necessary to balance the power losses and prevent it from cooling down.

The Lawson Criterion states that the product of temperature T, ion density n, and confinement time τ_{e} (quantity linked to the power losses) should exceed a certain value to ensure ignition conditions and thus guarantee zero external heating power requirements. This correlation is graphically represented in Fig.1 where the energy $[keV]$ is reported on the x-axis.

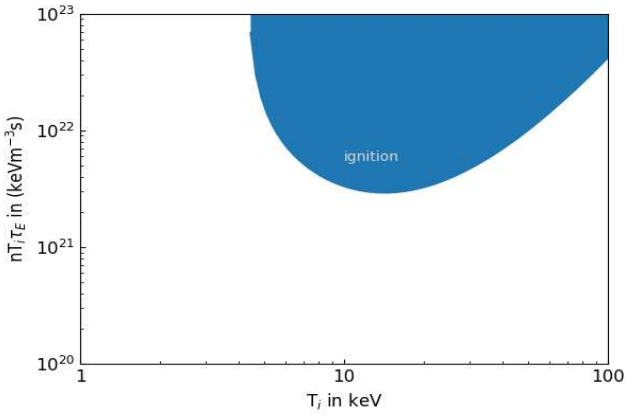

Figure 1: Lawson Criterion illustration: in blue it is represented the region where the ignition take place and no external heating is required.

The concept of ignition condition can also be expressed through an important parameter known as Energy Gain, which is defined as follows

$$Q = \frac{P_{\mathrm{th}}}{P_{\mathrm{H}}} \tag{4}$$

Depending on the value of Q we have the following conditions:

- For $Q < 0$, the energy used to heat up the plasma is higher than that produced by the nuclear reaction;
- For $Q = 1$, we have the so-called break-even condition, and so the power supply to the plasma is equal to the one produced by the reaction;
- For $Q > 1$, the energy used to heat up the plasma is lower than that produced by the nuclear reaction. The higher the value of Q the closer we are to the ignition condition defined by a value of $Q = \infty$ ($P_{\mathrm{H}} = 0$).

Nowadays, the best result achieved is $Q = 0.67$ by the JET experiment. The goal of ITER is to reach a value of $Q = 10$.

1.2 Neutral beam injection

Nuclear fusion reactions require a very high temperature to occur, at least 150 million degrees. The heat provided by ohmic effect, resulting from the strong currents flowing in the plasma in Tokamak configuration, required for its own equilibrium, is not sufficient to reach this goal alone. Therefore, additional heating systems are crucial for ITER, with NBI (Neutral Beam Injection) standing out as its primary solution.

The injection of neutral particles from negative ions is a well-known and widely used method to heat plasma confined within a magnetic field. The real challenge is to implement this technology for ITER, which requires energy, power, and continuity at parameters never reached before.

The research and development for the NBI system are carried out in Padova, at Consorzio RFX, within the NBTF project (Neutral Beam Test Facility).

To generate neutral particles at high energies, negative hydrogen or deuterium ions are extracted from a "plasma source" and accelerated up to an energy of 1 MeV by means of electrostatic fields. These particles are then neutralized to allow them to pass through the confinement magnetic field and collide with the plasma ions. The kinetic energy possessed by the former is thus transferred to the latter, heating up the plasma.

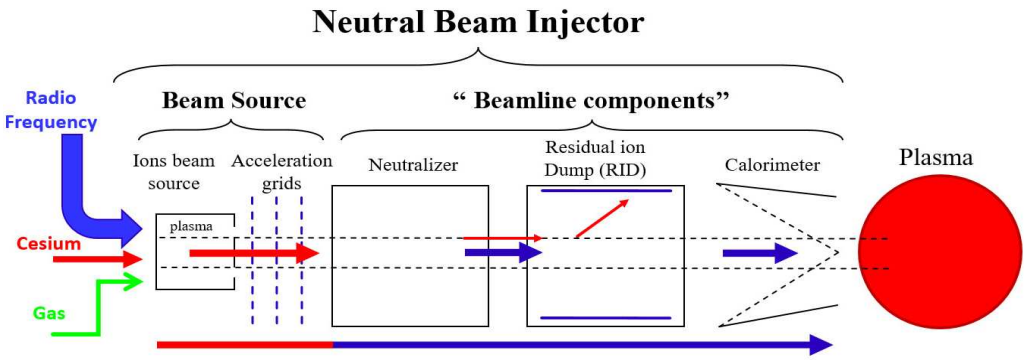

Figure 2: NBI Operation Illustration.

There are two test prototypes developed at the NBTF facility:

- SPIDER (Source for Production of Ion of Deuterium Extracted from Rf plasma), which is the prototype of the ion source and a first stage of acceleration;
- MITICA (Megavolt ITER Injector & Concept Advancement), which is the prototype of the entire neutral beam injector.

1.3 SPIDER

SPIDER is the 1:1 scale prototype of the negative ions source of the neutral beam injector (NBI) for the ITER experimental thermonuclear fusion reactor. It represents the biggest negative ions source and the apex of the physics and technological research in this sector. It is essentially composed by a vacuum vessel which houses:

- A container with 8 RF driver where a 1MHz radiofrequency current is used for the plasma generation;
- An electrostatic accelerator composed by three grids at different electric potential:
    1. Plasma grid:it divides the ions source from the accelerator, allowing, with the use of Cesium, the selection of negative particles;
    2. Extraction grid: allow the negative ions to be extracted and, thanks to its particular magnetic configuration, it deflects the electrons to impinge on the grid itself;
    3. Grounded grid: it allows the acceleration of negative ions up to 100 keV in a beam intercepted by a calorimeter.
- diagnostic systems, among which, particularly important are the two calorimeters STRIKE and BEAM DUMP.

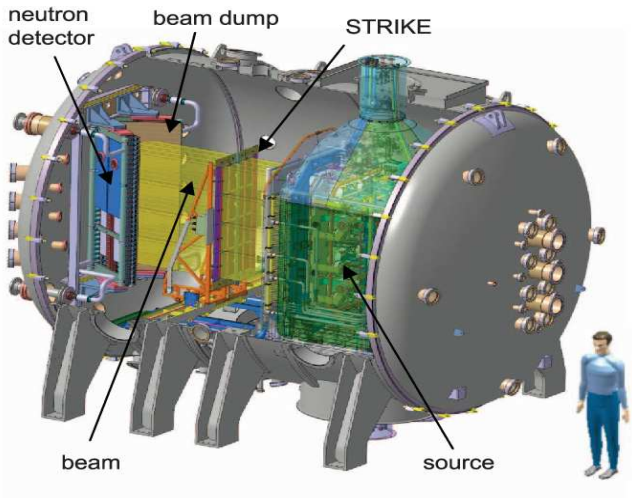

Figure 3: SPIDER illustration.

A relevant upgrade for SPIDER will be the installation of the "Beamlet Group Current Monitor" (BGCM) diagnostic, which will be used for the measurement of the beam current exiting the ground grid.

The current sensor signal, one for each of the 16 beamlet groups, will allow the measurement of the total beam current, and, in addition, the assessment of its uniformity.

The technology of the so-called Direct Current Current Transformer (DCCT) is considered the most promising for this type of current sensor, in terms of sensitivity, robustness, and immunity to disturbances.

2 DCCT Sensor

Among the various current sensor devices, DC Current Transformers (DCCTs) represent a very promising technology for the detection of the beam current at the exit of the ground grid. Unlike commonly used devices like Faraday cups, DCCTs allow non-intrusive measurement of beam currents through magnetic field coupling rather than charge collection.

This technology has been extensively studied by particle physicists and engineers for decades, providing very accurate current measurements of the high kinetic energy beam current (typically in the MeV range) generated at particle accelerators.

The principle of operation for DCCTs relies on the fluxgate magnetometer technique, a well-established technology widely used for magnetic field measurement. The conventional setup for a DCCT is depicted in Fig.4 and primarily consists of:

- Two symmetrical toroids which represent the core of the sensor;
- A modulator circuit;
- A demodulator circuit;
- A feedback circuit.

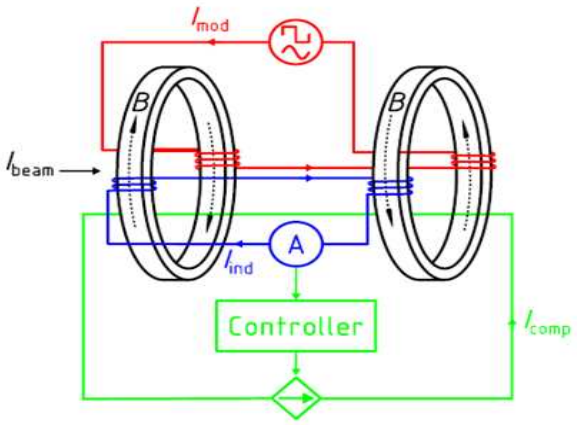

Figure 4: DCCT Sensor Setup.

In this configuration, the modulator circuit induces magnetic saturation in the two cores with a π phase shift. When a DC current flows through the cores, it causes an asymmetric shift in the generated magnetic fluxes. The resulting combination of these two fluxes exhibits a behaviour that is directly proportional to the amplitude of the DC current.

The feedback circuit is used to compensate for the DC current, enabling a direct measurement of it and allowing a wider measurement range by operating close to zero flux.

2.1 Fluxgate technology

Fluxgate magnetometers are used for measuring the magnitude and direction of a DC or low-frequency AC magnetic field. A fluxgate magnetometer typically consists of a ferromagnetic core around which two coils are wound. One coil is used to magnetize the core (excitation coil), and the other is used to detect changes in the magnetic field (pickup or detection coil).

The principle of operation exploits the magnetic properties of ferromagnetic materials. When a magnetic field is applied to a material, the overall magnetic field inside that material results from the combination of two factors: the applied (or excitation) magnetic field, and the magnetic field generated by the material in response. The nature and magnitude of the material's response are determined by its magnetic permeability μ. Based on this, substances can be categorized into three main types:

- Diamagnetic substances ($\mu < \mu_0$);
- Paramagnetic substances ($\mu \approx \mu_0$);
- Ferromagnetic substances ($\mu \gg \mu_0$).

Ferromagnetic materials exhibit a strong response to an external magnetic field, becoming strongly magnetized in the direction of the field. This behaviour is represented by their magnetization characteristic obtained applying a variable excitation field to the specimen (Fig.5).

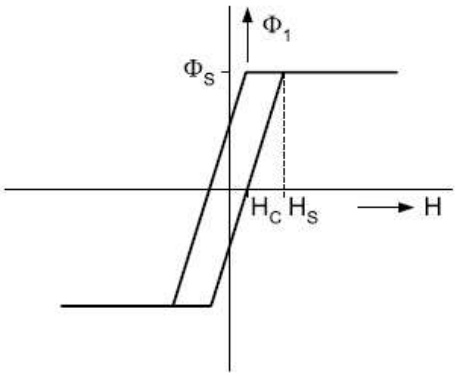

Figure 5: Hysteresis loop: ϕ is the magnetic flux, H is the excitation field.

For a closed magnetic circuit made of a ferromagnetic material, if a variable excitation magnetic field is applied, the idealized hysteresis loop of one-half of the sensor is identical to the magnetization characteristics of the material itself. When an external DC magnetic field is present, it distorts the hysteresis loop in the two halves in different ways:

- In one core leg, excitation and external field are aligned. Under this hypothesis, we reach the saturation sooner, that is the condition in which the material cannot be further magnetized. The saturation increases the magnetic reluctance, which gates or limits the flux in this part of the core;
- In the other half, excitation and external field are not aligned and, due to the gating effect on the other half, the effective permeability is decreased.

In addition, the characteristic is shifted by the external field along the H axis as is depicted in Fig.6; the characteristic for the second half-core is symmetrical with respect to the ϕ axis.

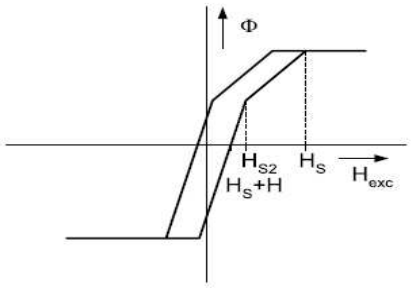

Figure 6: Distorted hysteresis loop.

By summing up these two loops, we obtain the transfer function (Fig.7) which exhibit a linear relationship with the intensity of the measured DC magnetic field. This linearity is preserve up to field intensity, for which the whole sensor becomes saturated.

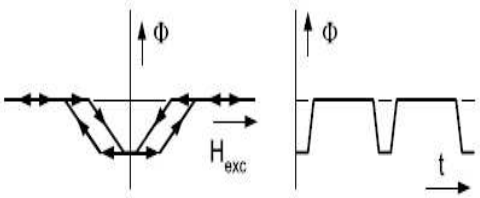

Figure 7: Transfer function obtained by the combination of the two distorted hysteresis loops.

The gating mechanism can be extended to the case of a two cores sensor as depicted in Fig.8.

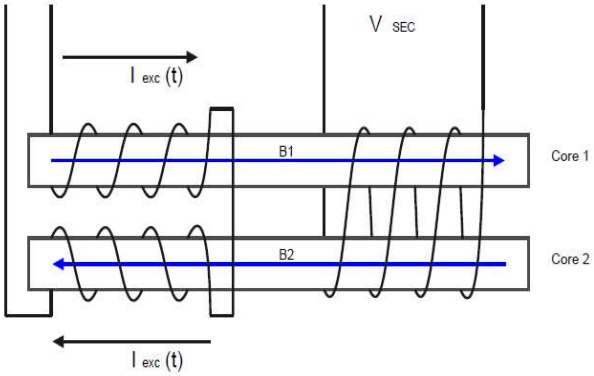

Figure 8: Two cores setup of a DCCT sensor.

The sensor consists of two identical cores represented by the two ferromagnetic bars, an excitation coil and a pick-up coil. Drive windings are connected in series and wound in opposite direction allowing the generation of opposite magnetic fields in the two cores.

By applying an AC excitation current, in absence of an external DC magnetic field, cores are saturated in both directions for an equal interval of time of the excitation period. The two fluxes from the two cores will exactly cancel out and no voltage will be induced in the pick-up coil Fig.9.

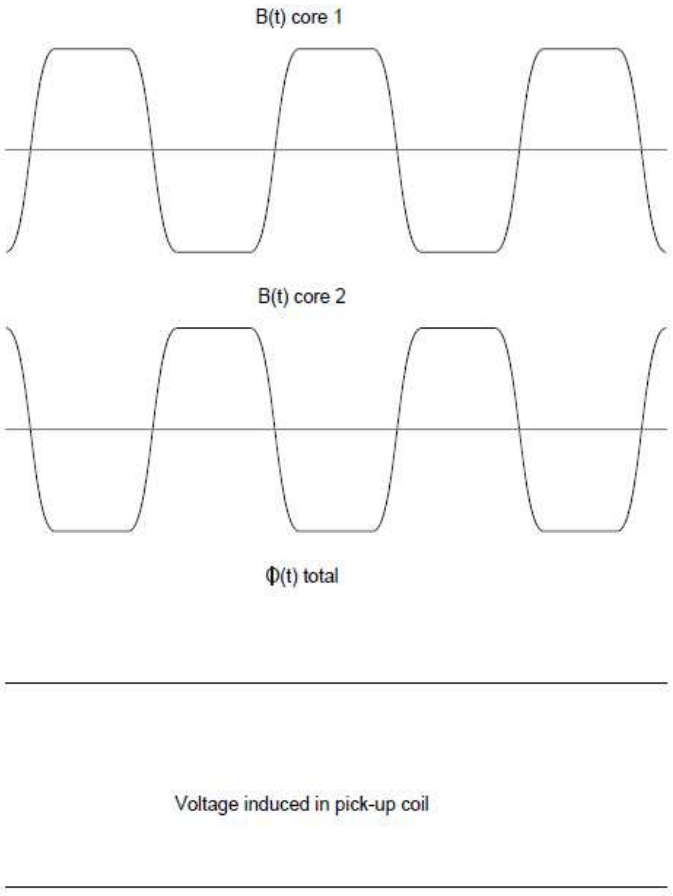

Figure 9: Characteristics of the magnetic field B, magnetic flux ϕ and pickup voltage with zero external field applied.

In reality, small variations of the cores' characteristics lead to a mismatch that makes the induced voltage not exactly equal to zero.

When an external DC magnetic field is applied, the time spent in one of the two saturations will increase and a pick-up signal will arise due to the relative shifts of the flux changes in each core Fig.10

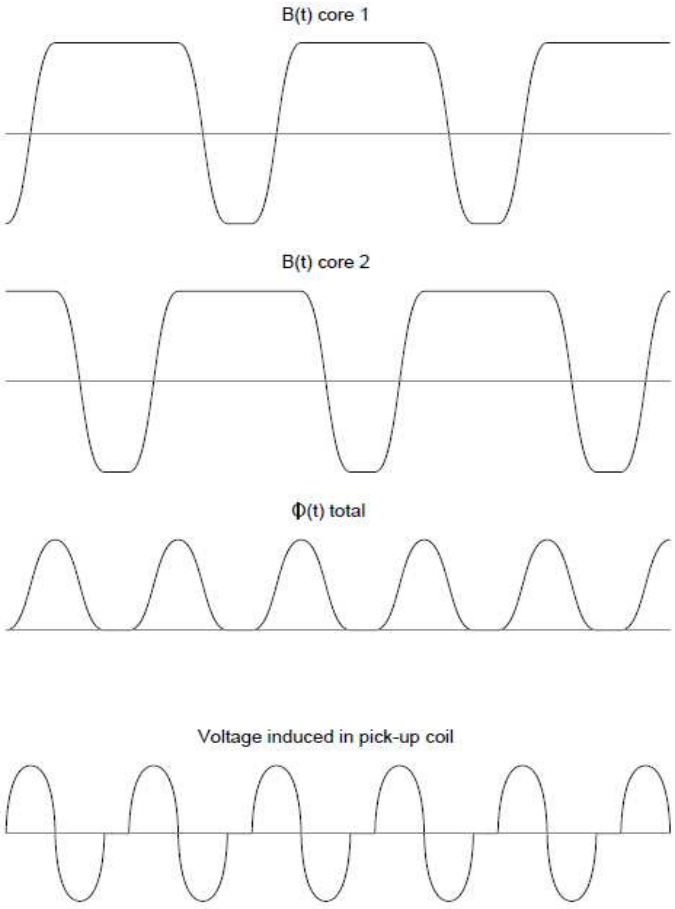

Figure 10: Characteristics of the magnetic field B, magnetic flux ϕ and pickup voltage with an external field applied.

The output signal of the pick-up coil (voltage and current detection are in use) contains odd and even harmonics of the fundamental drive frequency. The even harmonics are proportional to the external magnetic field along the magnetic axis of the sensor. The odd harmonics constitute the feed-through signal coupled from the drive coil and the soft magnetic core to the pick-up coil. Double cores (either double rod or ring-core) fluxgate allows the reduction of the large signal of the excitation frequency at the sensor output, and are normally used for precise measure.

2.2 Redout electronics

By applying an AC excitation signal, the sensor's core is periodically saturated in both polarities. This causes the core permeability to change, modulating the flux associated with the DC magnetic field, which can then be measured. The information related to the static magnetic field is contained in the second (and also higher even) harmonics of the excitation frequency. To extract this information, a number of techniques have been developed:

- Second Harmonic Method

  The second-harmonic detection of the output voltage is the most frequently used method. A phase-sensitive detector (PSD) filters out the fundamental component of the output voltage and amplifies its second-harmonic component. A low-pass filter can then be used to effectively smooth the signal and remove high-frequency noise.

- Non-selective Detection Method

  Different non-selective detection methods processing the output signal in the time domain have been developed as an alternative to the second-harmonic detection:

  - Peak Detection Method

    The peak detection method is based on the relationship between the voltage output peaks and the intensity of the measure magnetic field. The difference between positive and negative peaks of the output voltage changes with the intensity of the magnetic field and is equal to zero for a null field. This relationship may be linearly dependent on the measured field within a narrow interval;

  - Sampling Method

    The sampling method is based on the fact that the instantaneous value of the excitation current at the time of zero-crossing of the core induction depends on the measured field.

The practical implementation of these techniques depends on the type of fluxgate employed: Analog fluxgate or Digital fluxgate.

For the realization of the DCCT sensor, the second-harmonic detection has been investigated.

2.2.1 Analog fluxgate

Fig.11 shows the block diagram of a typical analog magnetometer working on the second-harmonic principle. The generator (GEN) serves the dual purpose of generating the excitation signal at frequency f and producing the $2f$-squarewave reference signal for the PSD.

The potential presence of first harmonic and other unwanted signals at the sensor output, which are sometimes too high for the PSD, lead to the need to preamplify the signal and, sometimes, filter it through a band-pass filter.

To achieve adequate amplification, an integrator (INT) is introduced into the feedback loop. This loop signal is then directed back to the feedback coil, thereby expanding the linear range of the sensor.

Furthermore, additional feedback current generated by the digitally controlled current source may be introduced to further extend the instrument's range.

The dynamic range of the basic analog feedback magnetometer may be 120 dB, which is sufficient for most of the applications; it allows for the construction of an instrument with 100 μT range, making it possible to measure the Earth's field with 0.1-nT resolution.

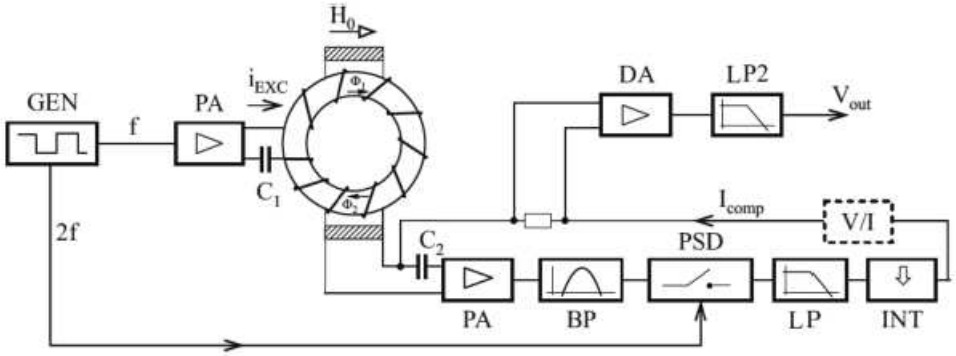

Figure 11: Block diagram of a typical analog magnetometer working on the second-harmonic principle.

2.2.2 Digital fluxgate

In a digital fluxgate magnetometer, the field information extraction from the sensor output and the calculation of the feedback signal are done in the digital domain. The reduced number of analogue parts allows to achieve a sensor which:

- Is more robust against changes of electronics temperature and supply voltages;
- Is less sensitive to electromagnetic disturbances;
- Features higher flexibility of the instrument operation.

Fig.12 shows the typical setup of a digital fluxgate magnetometer.

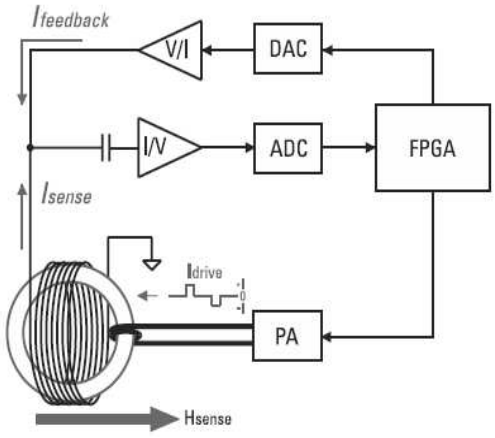

Figure 12: Digital fluxgate setup.

This sensor electronics concept reduces the number of analogue components by digitizing the output signal of the pick-up coil directly after the input amplifier. Thus, an ADC is necessary to move from the analog to digital domain. Demodulation algorithms are then implemented in either a field-programmable gate array (FPGA) or in a digital signal processor. The feedback signal is generated by a DAC controlled and updated by the digital processing unit.

A digital fluxgate system offers enhanced performance over traditional demodulation techniques and introduces novel capabilities:

- Digital phase-sensitive detection enables the consideration of not only the second-harmonic component but also higher even harmonics. This expanded harmonic analysis potential can enhance sensitivity and reduce noise;

- An alternative approach in digital fluxgate magnetometry involves integrating the control loops of a $\Sigma\Delta$ modulator with the conventional fluxgate magnetometer readout electronics in order to achieve a new magnetometer design that provides direct digital output without the use of a separate analogue-to-digital converter chip.

  Sigma–delta modulation technique is a very cost effective and robust type of analogue-to-digital conversion which is particularly useful when high resolution is required.

  The simplest sigma–delta modulator is a first-order loop which consists of an integrator and a comparator (two-level or single-bit quantizer respectively) in the forward path and a single-bit DAC in the negative feedback (Fig.13).

  The basic principle involves oversampling the analog signal, quantizing it into a 1-bit digital signal (a stream of ones and zeros), and then using a feedback loop to continuously adjust the output based on the difference between the input and the quantized output. This feedback loop operates at a high frequency and effectively shifts quantization noise out of the band of interest, resulting in a high-resolution digital representation of the original signal.

  The high-frequency quantization noise is then removed by means of a digital decimation (low-pass) filter operating at the output of the sigma–delta modulator.

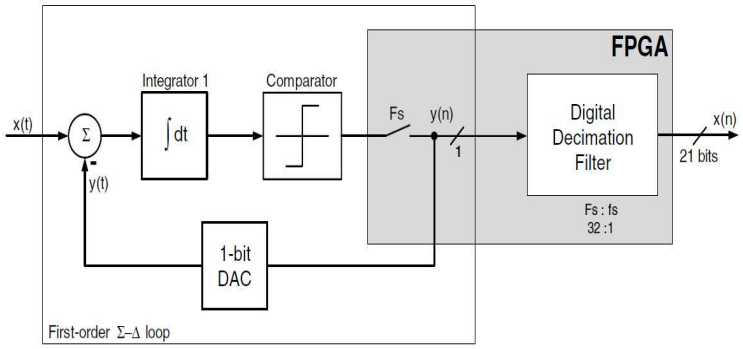

Figure 13: Block diagram of a first-order sigma–delta converter.

2.3 Feedback control

Sensor second-harmonic output voltage and external magnetic field manifest a proportional behaviour up to a certain intensity value of the field. As the sensor itself usually has a linear range limited to typically 1μT, fields larger than that have to be compensated.

The demodulated signal is used to generate a set point value for the controller unit, which in turn triggers the compensation current $\mathrm{I_{comp}}$ which flows through both cores balancing the beam current $\mathrm{I_b}$ and allowing operation close to zero flux.

The compensation current represents a direct measurement of the beam current:

$$I_{\mathrm{b}} = I_{\mathrm{comp}} + \Delta I \tag{5}$$

The discrepancy ΔI primarily arises from variations among the cores and the inherent noise level in the electrical circuitry. This disparity can be reduced through system calibration and the implementation of suitable filtering techniques on the induced signal.

The feedback field should be homogeneous and therefore a large feedback coil is required. In simple magnetometers, the pickup coil also serves for the feedback, but this requires some trade-offs with the readings of the output voltage. Thus, in precise magnetometers, the two pickup coils and the compensation coils are separated.

The generation of the compensation current for the DCCT sensor has been implemented using a synchronous demodulation approach together with a PID controller.

2.3.1 Synchronous demodulation

The linear behaviour between the pickup voltage and the beam current has been verified for the case of the real DCCT sensor. As depicted in Fig.14 the proportionality links the intensity of the current to the mean value of the output voltage. In order to extract this information, a synchronous demodulation approach is adopted.

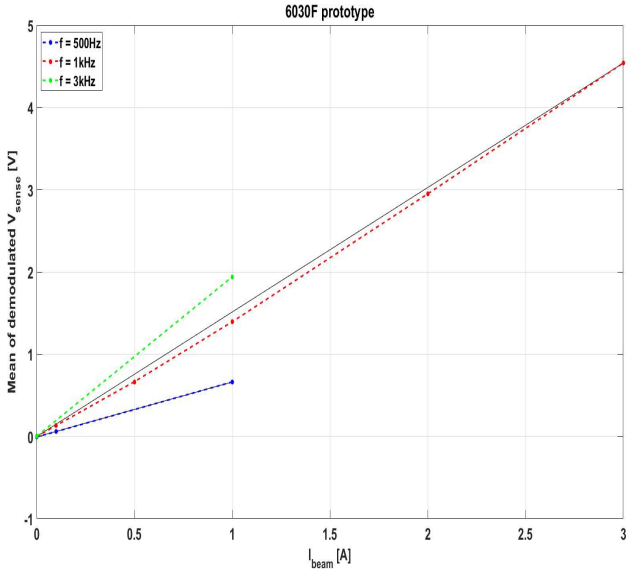

Figure 14: Relationship between mean pickup voltage and beam current intensity for the DCCT sensor.

Synchronous demodulation is implemented to reduced the flicker noise usually associated to the measurement of a DC or low-frequency signal. The average power of the flicker noise is inversely proportional to the frequency of operation; that's why it is also known as 1/f noise. The idea is to use a modulating signal to move the output signal beyond the 1/f noise corner frequency, preserving the information of the DC value. This allow to move from the flicker noise region to the thermal noise region as depicted in Fig.15.

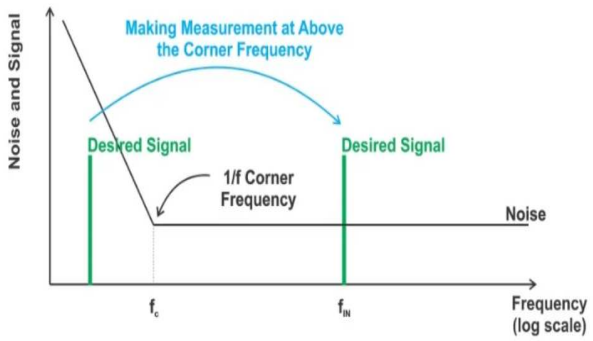

Figure 15: Noise Frequency Response.

In the specific case of a DCCT sensor, the output voltage can be represented by means of its Fourier Series as follows:

$$V_{\text{pickup}}(t) = \sum_{k=1}^{\infty} V_{\text{k}} \sin(kwt) \tag{6}$$

The demodulation of the DC value associated with the second-harmonic component $V_{\text{2-harmonic}} = A \sin(2\pi f_{2,\text{h}} t)$ is carried out as follow:

$$V_{\text{A}} = V_{\text{2-harmonic}} \times B \sin(2\pi f_{2,\text{h}} t + \Phi) = \frac{1}{2} AB \cos(\Phi) - \frac{1}{2} AB \cos(4\pi f_{2,\text{h}} t + \Phi) \tag{7}$$

By multiplying $V_{\text{2-harmonic}}$ to a sinusoidal signal with the same frequency (twice the excitation frequency) but different phase, the result is a combination of two factor: a first DC term, and a second term at twice the input frequency. With the implementation of a low-pass filter it is possible to eliminate the AC term, and so to have:

$$V_{\text{A,filtered}} = \frac{1}{2} AB \cos(\Phi) \tag{8}$$

The results is a DC value that is proportional to the intensity of the output voltage second-harmonic component (A) and is a function of the phase difference between the two signals (Φ). In order to remove the dependency on the phase difference, the same calculation can be performed considering

a cosine signal:

$$V_{\mathrm{B}} = V_{\text{2-harmonic}} \times B\cos\left(2\pi f_{2,\mathrm{h}} t + \Phi\right) = \frac{1}{2}AB\sin\left(\Phi\right) - \frac{1}{2}AB\sin\left(4\pi f_{2,\mathrm{h}} t + \Phi\right) \tag{9}$$

After the filtering, the DC term associated to V_2 is:

$$V_{\mathrm{B,filtered}} = \frac{1}{2}AB\sin\left(\Phi\right) \tag{10}$$

We can thus remove the phase dependence by taking the square root of the sum of the squares of $\mathrm{V}_{2,\mathrm{filtered}}$ and $\mathrm{V}_{1,\mathrm{filtered}}$ as follows:

$$V_{\mathrm{filtered}} = \sqrt{{V_{\mathrm{A,filtered}}}^2 + {V_{\mathrm{B,filtered}}}^2} = \frac{1}{2}AB \tag{11}$$

The multiplication of the signal of interest (second-harmonic component) to a sinusoidal signal of the same frequency is equivalent to implement a phase-sensitive rectification. The multiplication modifies the frequency spectrum mainly converting the second harmonic into a direct component.

Theoretically, following low-pass filtering, the average of the phase-sensitive output is mainly proportional to the amplitude of the second harmonic of the sensor output, which is the majority of the fluxgate signals:

$$\overline{v}(t) = \frac{\omega}{\pi}\int_0^{\frac{\pi}{\omega}} \frac{1}{2(2k+1)} V_{2(2\mathrm{k}+1)} \approx \frac{4}{\pi}A \tag{12}$$

2.3.2 PID controller

A digital PID controller is used to control the compensation current generator within the feedback loop. An error value $e(t)$ is defined as the difference between a desired set-value (theoretically zero) and the output of the demodulation process. The PID implement a correction based on the proportional, integrative and derivative term of $e(t)$.

Defined the discrete time as $t[kT_{\mathrm{s}}] = t^{\mathrm{k}}$ ($\mathrm{T_s}$ sampling time), and the discrete error as e^{k}, the controller algorithm in the discrete domain is implemented as follow:

$${V^{\mathrm{k}}}_{\mathrm{DAC}} = {V^{\text{k-1}}}_{\mathrm{DAC}} + (k_{\mathrm{p}} + \frac{k_{\mathrm{i}}T_{\mathrm{s}}}{2} + \frac{k_{\mathrm{d}}}{T_{\mathrm{s}}})e^{\mathrm{k}} - (k_{\mathrm{p}} - \frac{k_{\mathrm{i}}T_{\mathrm{s}}}{2} + \frac{2k_{\mathrm{d}}}{T_{\mathrm{s}}})e^{\text{k-1}} + \frac{k_{\mathrm{d}}}{T_{\mathrm{s}}}e^{\text{k-2}} \tag{13}$$

Where:

- V_{DAC} refers to the analog voltage, output of the DAC, used to drive the current generator;
- k_p denotes the proportional gain;
- k_i denotes the integral gain which multiply the integral term defined by the trapezoidal rule;
- k_d denotes the derivative gain which multiply the differentiation term approximated by the backward Euler method.

The controller algorithm is implemented in parallel form and fully recursively to inhibit the wind-up effect caused by the integral part and to generally enhance control performance.

3 Sensor Model

The development of a sensor model has been necessary to validate and assess the various demodulation techniques adopted before their actual implementation in Arduino; the project was carried out using PSIM, a simulation software designed for the analysis and design of power electronics and motor drive systems. It provides engineers and researchers with a comprehensive platform for modelling, simulating, and optimizing various power electronic circuits and control strategies. PSIM also supports real-time simulation and hardware-in-the-loop (HIL) testing, making it suitable for both simulation-based design and real-world implementation.

3.1 Pickup voltage signal

The curves depicted in Fig.16 represents the trends of the excitation voltage and current, and the pickup voltage for a real DCCT sensor having the following characteristics:

- Excitation circuit: the setup consists of a Siglent SDG2122X waveform generator, AE Techron 7234 amplifier, and a 2:1 transformer to eliminate DC offset. This setup is employed to produce a sinusoidal voltage with a frequency of 500 Hz and an amplitude of 2 V;
- Modulator winding: 59 turn per core;
- Core materials: VITROVAC 6030F;
- Pick-up winding: 59 turn per core;
- Pick-up acquisition: the setup consists of a voltage differential probe in conjunction with a LeCroy WaveSurfer 44Xs oscilloscope;
- Compensation winding: 3 turn.

A schematic diagram of the sensor is depicted in Fig.17, while a corresponding illustration is provided in Fig.18.

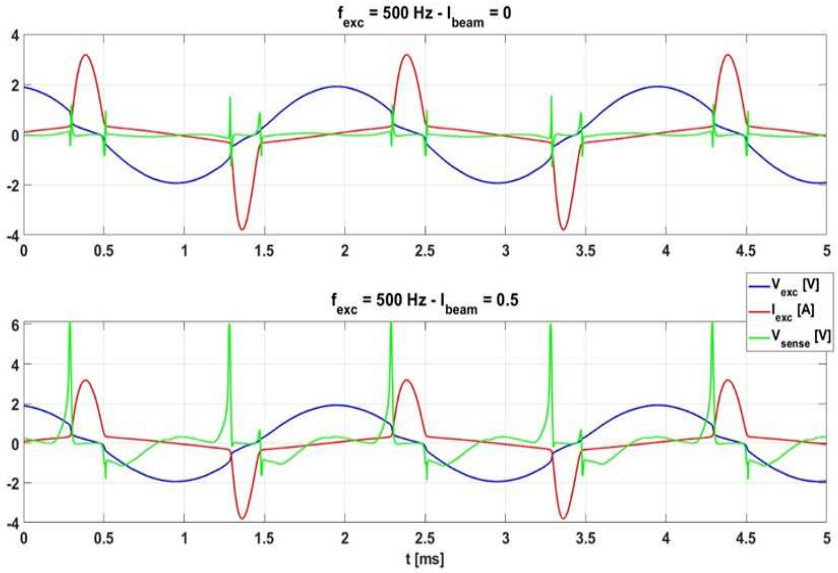

Figure 16: Pickup voltage characteristic (V_{sense}) of a DCCT sensor excited with a 500Hz sinusoidal voltage, sensing a beam current of 0.5 A.

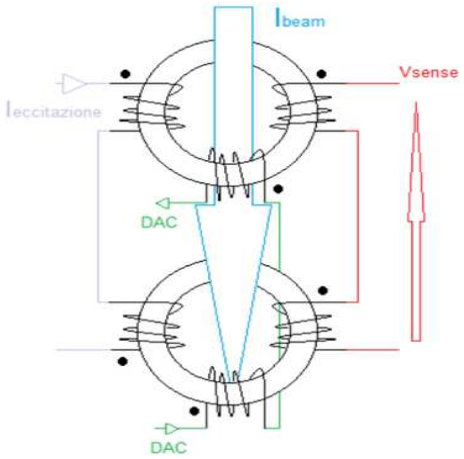

Figure 17: A simplified representation of the DCCT sensor in use.

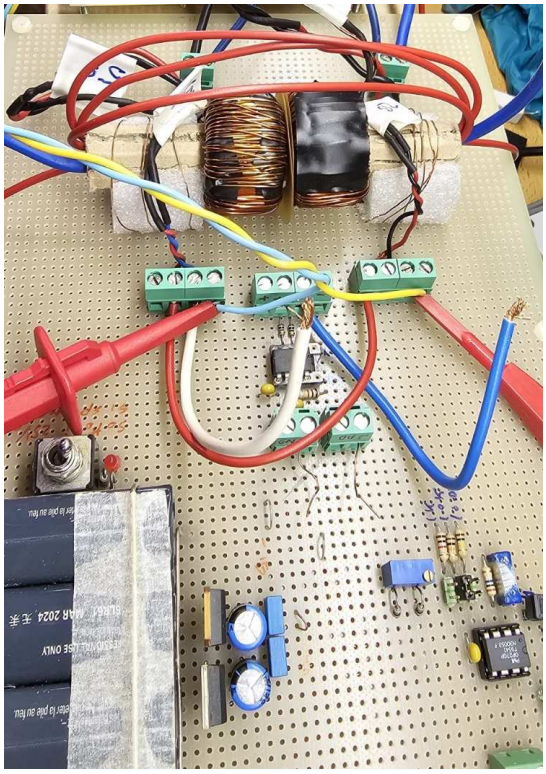

Figure 18: Photo of the DCCT sensor.

Based on the sensor specifics provided, a model was developed using PSIM. This model allows the extraction of the magnetic flux from the sensor core. In order to obtain the output voltage, differentiation of this signal has to be performed. Three distinct techniques of differentiation are evaluated:

1. Sensor Model 1

   In sensor Model 1, the derivative is performed by an ideal differentiator implemented through an ideal operational amplifier as depict in Fig.19. The relationship between the magnetic flux ϕ and the pickup voltage is described by the equation:

$$V_{\text{sense}} = -RC\frac{d\phi}{dt} \tag{14}$$

   where V_{sense} represents the pickup voltage, R is the resistance, C is the the capacitance and $\frac{d\phi}{dt}$ denotes the rate of change of magnetic flux

over time. The results of the simulation are illustrated in Fig.20 which depicts the trend over time of the pick-up voltage (V_{sense} in volts).

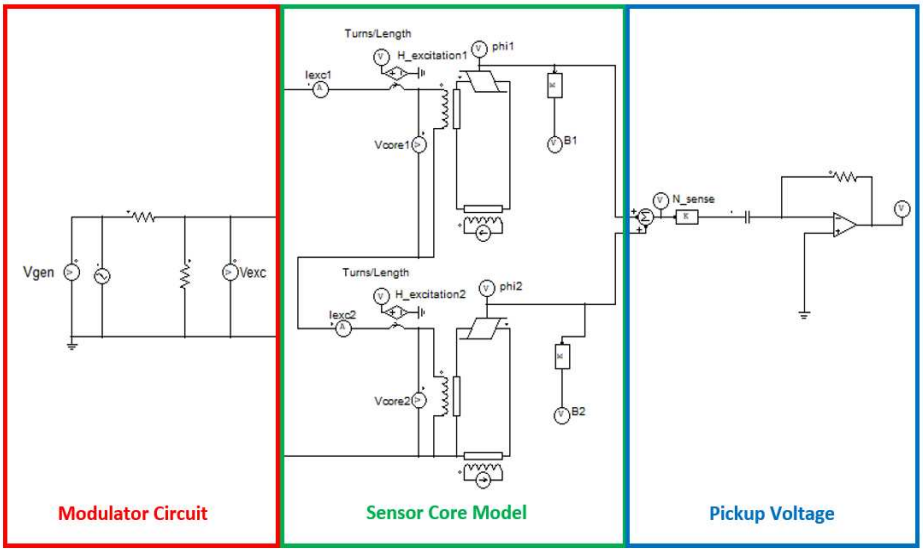

Figure 19: Sensor Model 1: PSIM circuit diagram of the proposed sensor system.

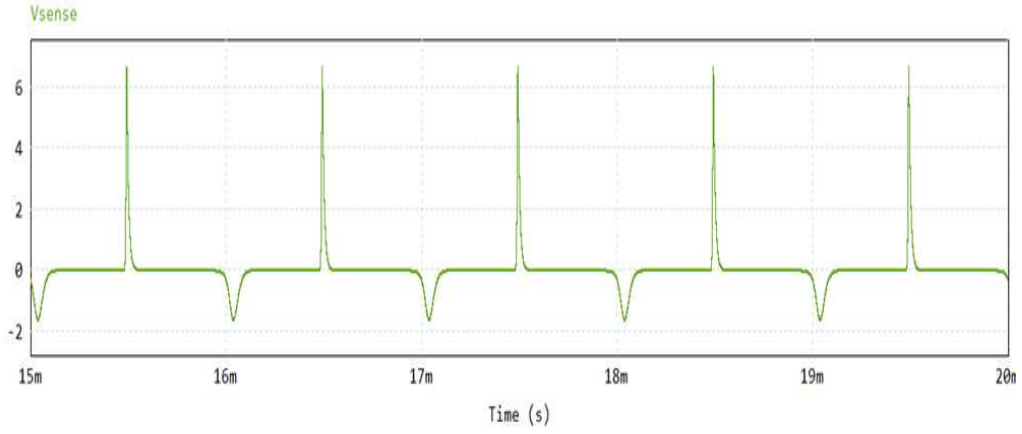

Figure 20: Model 1, plot of V_{sense}.

2. Sensor Model 2

   In Model 2, the derivative is performed using a "real differentiator" implemented through an ideal operational amplifier. The PSIM level-2 model of the capacitor includes leakage resistance, series resistance, and series inductance allowing the introduction of losses and disturbances at the pickup winding (Fig.21).

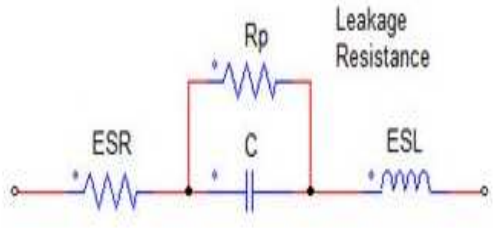

Figure 21: PSIM level-2 capcitor model. ESR represents the series resistance, Rp represents the leakage resistance and ESL represents the series inductance. For the simulation the following values was considered: ERS = 1 Ω; Rp = 0 (the resistor is ignored and is removed from simulation); ESL = 0.

The results of the simulation are reported in Fig.22

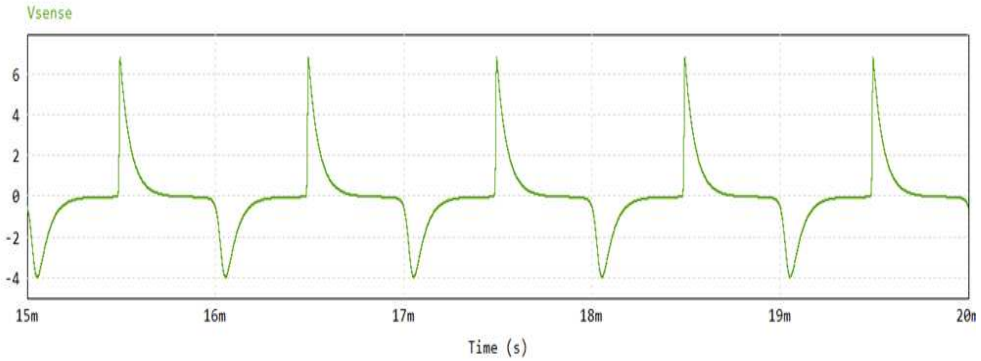

Figure 22: Model 2, plot of V_{sense}.

3. Sensor Model 3

In model 3, the derivative is performed using the d/dt PSIM block as depicted in Fig.23. The d/dt block implement the following mathematical equation:

$$V_0 = \frac{V_{\text{in}}(t) - V_{\text{in}}(t - \Delta T)}{\Delta T} \tag{15}$$

Where ΔT is the sampling time.

The results of the simulation are reported in Fig.24.

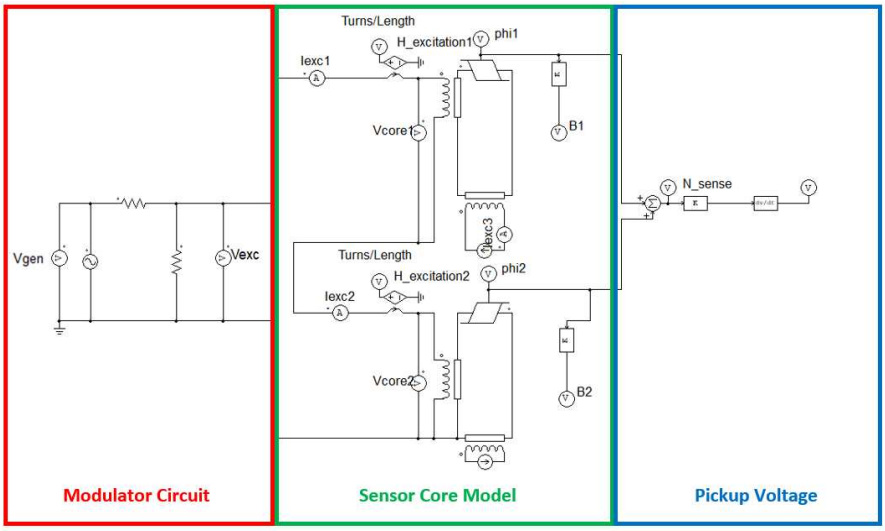

Figure 23: Sensor Model 3: PSIM circuit diagram of the proposed sensor system.

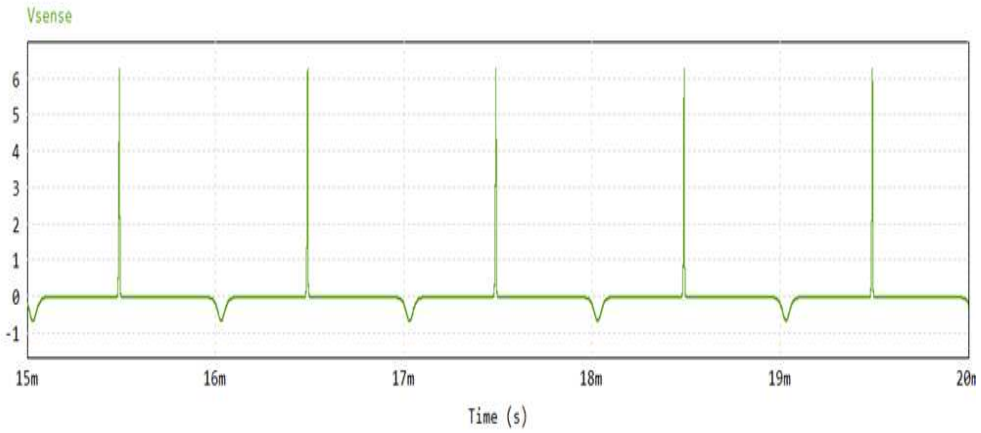

Figure 24: Model 3, plot of V_{sense}.

The model characteristics closely approximate the trend of the real sensor output voltage. Unlike Model 3, the introduction of power unit blocks (capacitor and operational amplifier) in Models 1 and 2 adds a load to the sensor core, which affects its linearity.

3.2 Model linearity investigation

A synchronous demodulation scheme was then implemented to the output voltage of each sensor model as depicted in Fig.25

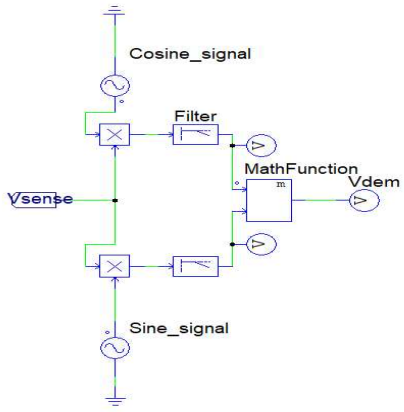

Figure 25: Synchronous demodulation scheme

The high frequency signal arising from the multiplication of Vsense to the sinusoidal signal, is then filter out by the low-pass filter, leaving a demodulated signal which oscillate around a DC value proportional to the intensity of the beam current (Fig.26). The average value around which the demodulated voltage oscillate has been calculated for different values of Ibeam and used to assess the linearity of the sensor model.

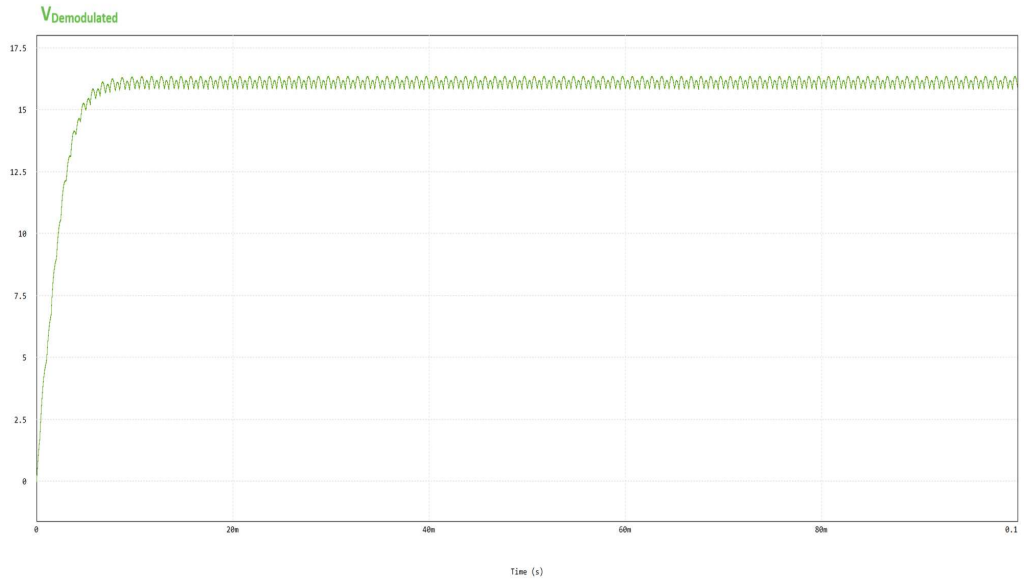

Figure 26: Demodulated voltage characteristic obtained for a $I_{beam} = 0.5A$

Based on the simulation results presented in table.27, a linear regression line was drawn using the Ordinary Least Squares method . The illustrations of Fig.28, Fig.29 and Fig.30, highlight the linearity between the beam current intensity and the average output voltage of the demodulation circuit.

Ibeam [A]	Model 1 Average demodulated output $V_{dem,average}$ [V]	Model 2 Average demodulated output $V_{dem,average}$ [V]	Model 3 Average demodulated output $V_{dem,average}$ [V]
0	0,000	0,0000	0,000
0,5	4,041	0,3415	4,129
1	8,074	0,6825	8,075
2	16,107	1,3608	16,102
3	23,863	2,0323	24,050
5	38,026	3,3500	39,653
10	60,633	6,4639	76,557

Figure 27: Average demodulated output voltage as a function of the beam current intensity

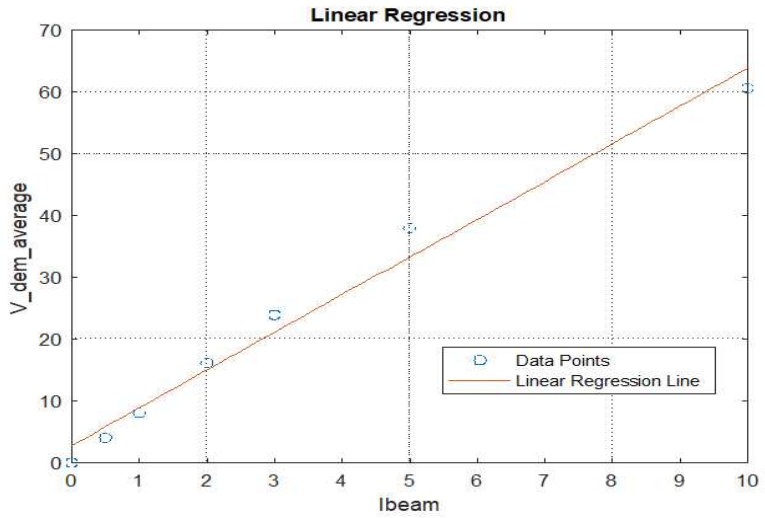

Figure 28: Illustration of the linear relationship between average demodulated output voltage of the DCCT and the intensity of the beam current for sensor Model 1.

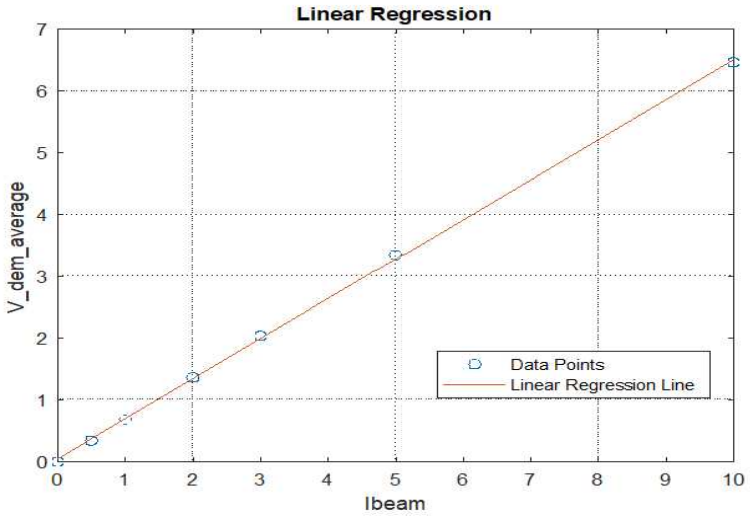

Figure 29: Illustration of the linear relationship between average demodulated output voltage of the DCCT and the intensity of the beam current for sensor Model 2.

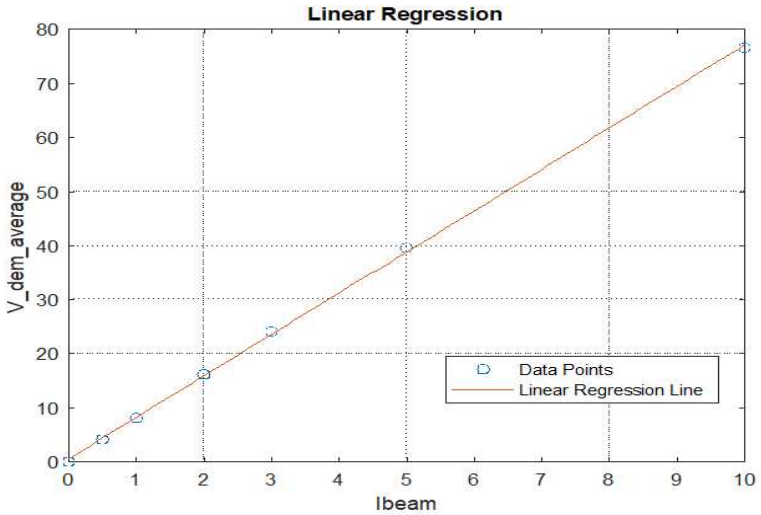

Figure 30: Illustration of the linear relationship between average demodulated output voltage of the DCCT and the intensity of the beam current for sensor Model 3.

Unlike model 1, the results of the simulation highlight the fact that the linear behavior is preserved up to values of 10 amperes for model 2 and 3.

3.3 Compensation current generation

Downstream the synchronous demodulation process, a PID controller implemented in parallel form has been used for compensation current generation. The compensation windings are connected in series as depicted in fig.31

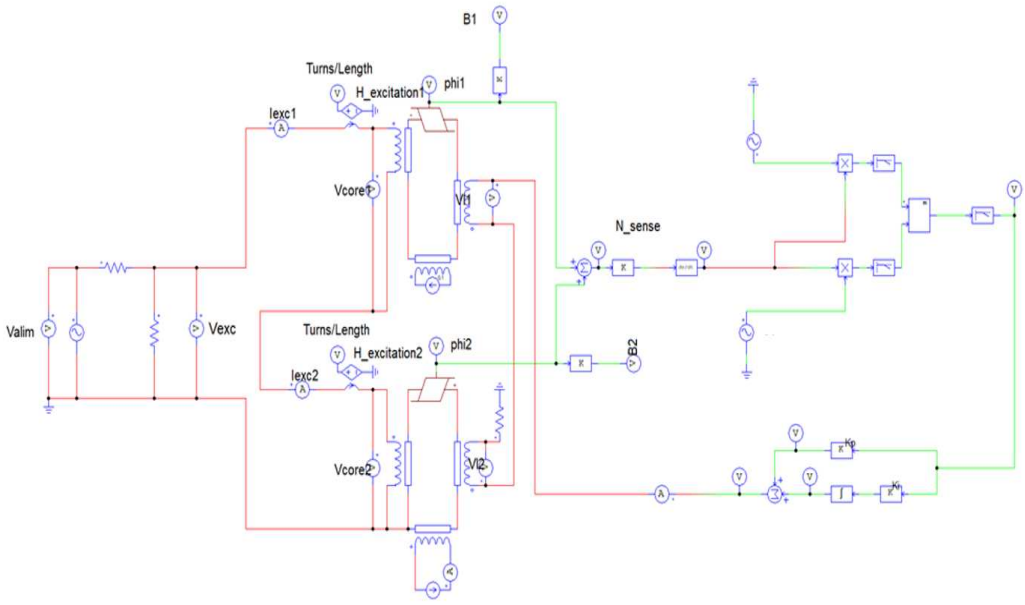

Figure 31: Closed-loop PSIM sensor model.

The simulation results depicted inFig.32 and Fig.33 were obtained using the parameters $k_p = 0.02$, $k_i = 3$, $k_d = 0$ and $I_{beam} = 0.1$ A. Model 3 was selected as the reference for evaluating the PID system response.

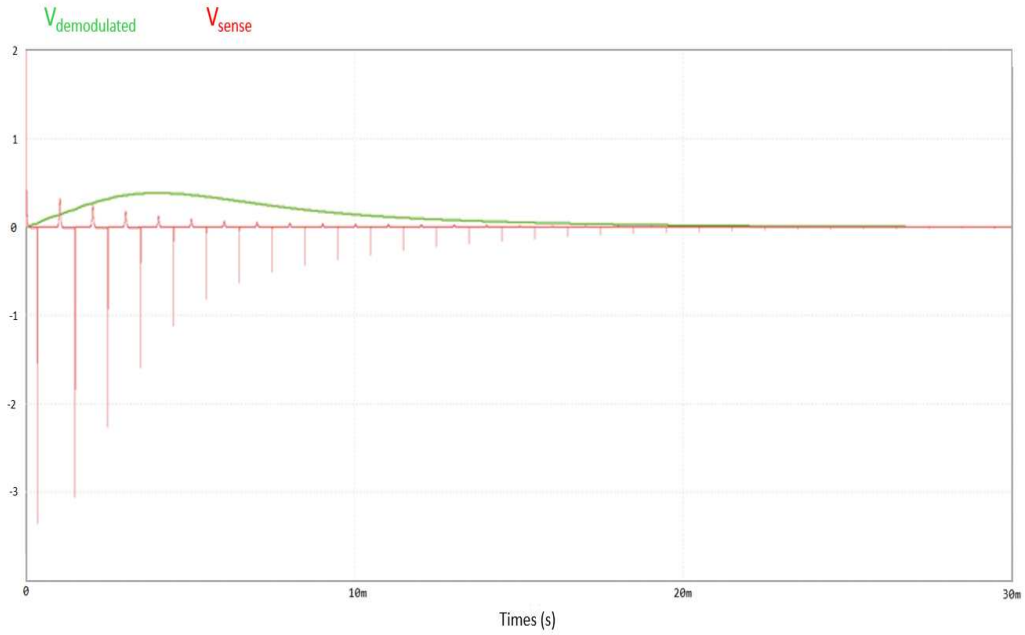

Figure 32: Pickup voltage (V_{sense}) and synchronous demodulation output signal ($V_{demodulated}$) characteristics for a closed-loop sensor model.

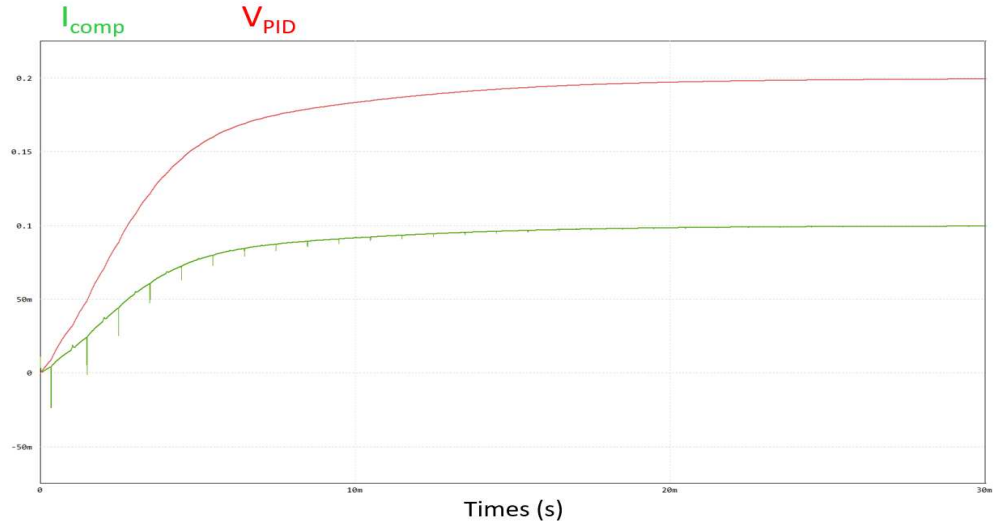

Figure 33: PID output voltage (V_{PID}) and current (I_{comp}) characteristics

The demodulated signal is fed to the PID which generate a compensation current in response. As expected, the feedback loop response stabilizes at a steady-state value where I_{comp} equals I_{beam}, and the sensor pickup voltage returns to zero flux.

3.4 Digital model

An additional model implementing algorithms for synchronous demodulation and digital PID control was then developed. A 12-bit ADC was used to sample the output voltage of the sensor. The digital implementation was achieved through the Simplified C Block, which allows to input C code directly without compiling. A C interpreter engine interprets and executes the C code at runtime. Through the Simplify C-block, it was possible to create a code that:

- Converts binary values outputted by the ADC into decimal values;
- Realizes digital synchronous demodulation. In particular, sine and cosine functions were defined by including the math.h library. Signal filtering is achieved using a first-order low-pass filter, defined as follows

$$y(k) = (1 - \alpha)y(k - 1) + \alpha u(k) \tag{16}$$

  Where:

  - y(k) is the the output of the filter at instant k;
  - α is a coefficient determined as follows:

$$\alpha = \frac{\Delta T}{\Delta T + TC} \tag{17}$$

    In which ΔT represents the ADC sampling time and TC is the time constant of the filter and is defined by the equation:

$$TC = \frac{1}{2\pi f_{\mathrm{t}}} \tag{18}$$

    With f_t, the cut-off frequency of the filter.
  - u(k) is the input signal

- Implements a digital PID controller (eq.13). Appropriate values for k_p, k_i, and k_d to ensure convergence of the feedback signal were determined by consulting data from various sources.

The sensor model circuit is depicted in Fig.34

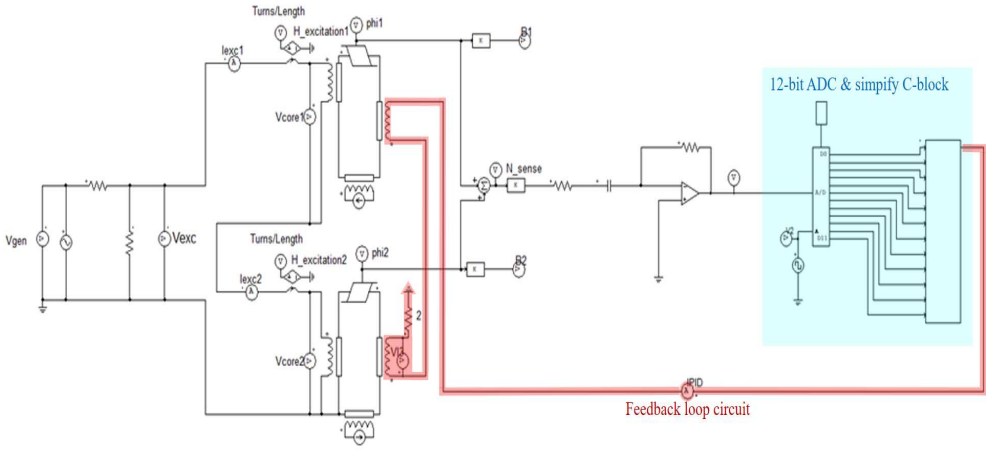

Figure 34: Digital PSIM model: In blue are highlighted the digital implementation components; in red the serial-connected feedback loop circuit.

The results of the simulations for the digital model reported in Fig.35 refers to a vlaue of $I_{beam} = 1$ A.

Figure 35: Closed-loop PSIM digital sensor model.

The digital control implemented through the Simplify C Block, generates a compensation current that stabilizes at a steady-state value near 1 A. The discrepancy between this steady-state value and the actual value of I_{beam} is attributable to the quantization error introduced by the 12-bit ADC.

4 Implementation

The signal processing and control techniques evaluated in the PSIM models have been applied in the physical implementation of the electronic components for the DCCT sensor prototype used in beam current measurement in SPIDER. A microcontroller has been employed to oversee the electronic board responsible for voltage acquisition and control voltage generation.

4.1 Electronic board

The electronic board for signal acquisition and generation, comprises:

- A 12-bit ADC (MCP3202) with isolation, allowing a maximum sampling frequency of 100 ksps at a 5 V supply voltage. The quantities that can be acquired are:
  - The excitation current with a 0.2 Ω shunt on CH1
  - The induced voltage in the secondary winding, using a voltage divider (on CH0)
- A Dual 12-Bit voltage output isolated DAC (MCP4822), which drives a transistor amplifier (BC337) utilized for compensation current generation. The circuit diagram of the amplifier is depicted in Fig.36;

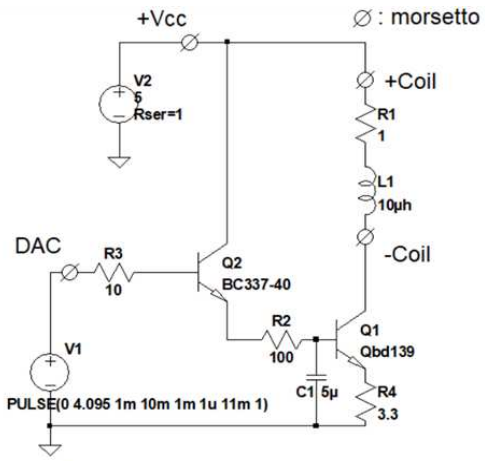

Figure 36: Transistor amplifier circuit. It allows the generation of a compensation current up to 500 mA.

The output of the DAC is directly taken from the connector P11, and in particular, CHA is used;

- A ESP32 microcontroller used for signal processing and managing communication with the ADC and DAC.

In this initial prototype, the excitation signal is generated by an external power amplifier fed with a sine wave voltage generated by a Siglent SDG2122X waveform generator.

Instead, it is possible to change the full scale of the acquisition by managing three levels of preamplification: x1, x10, and x100. By changing the jumper on the board it is possible to set the desired level of amplification. The corresponding illustration of the electronic board and DCCT sensor is provided in Fig.37.

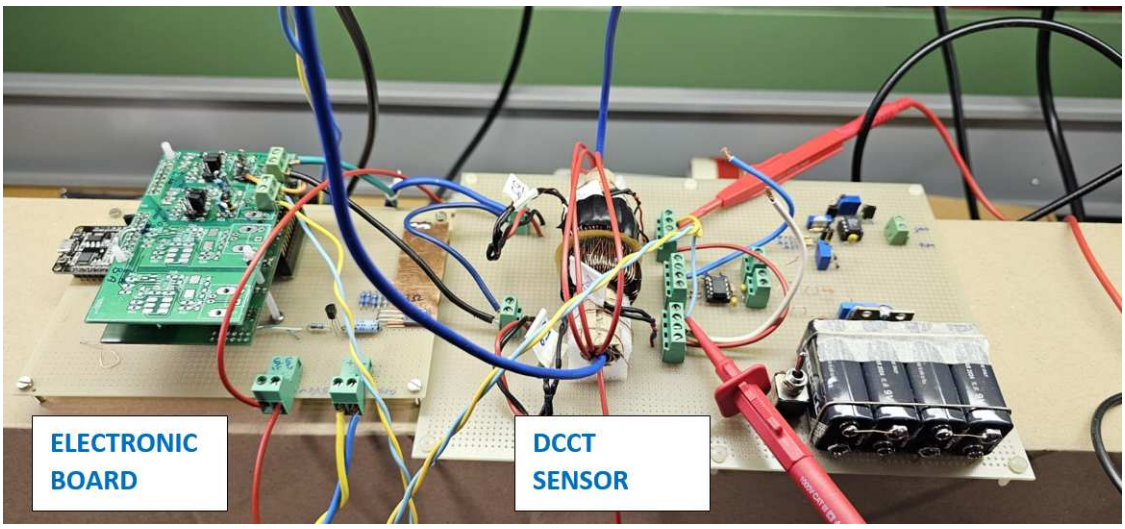

Figure 37: Photo of the DCCT sensor and the integrated electronic board.

Details of the electronic board connections are provided in the following pages.

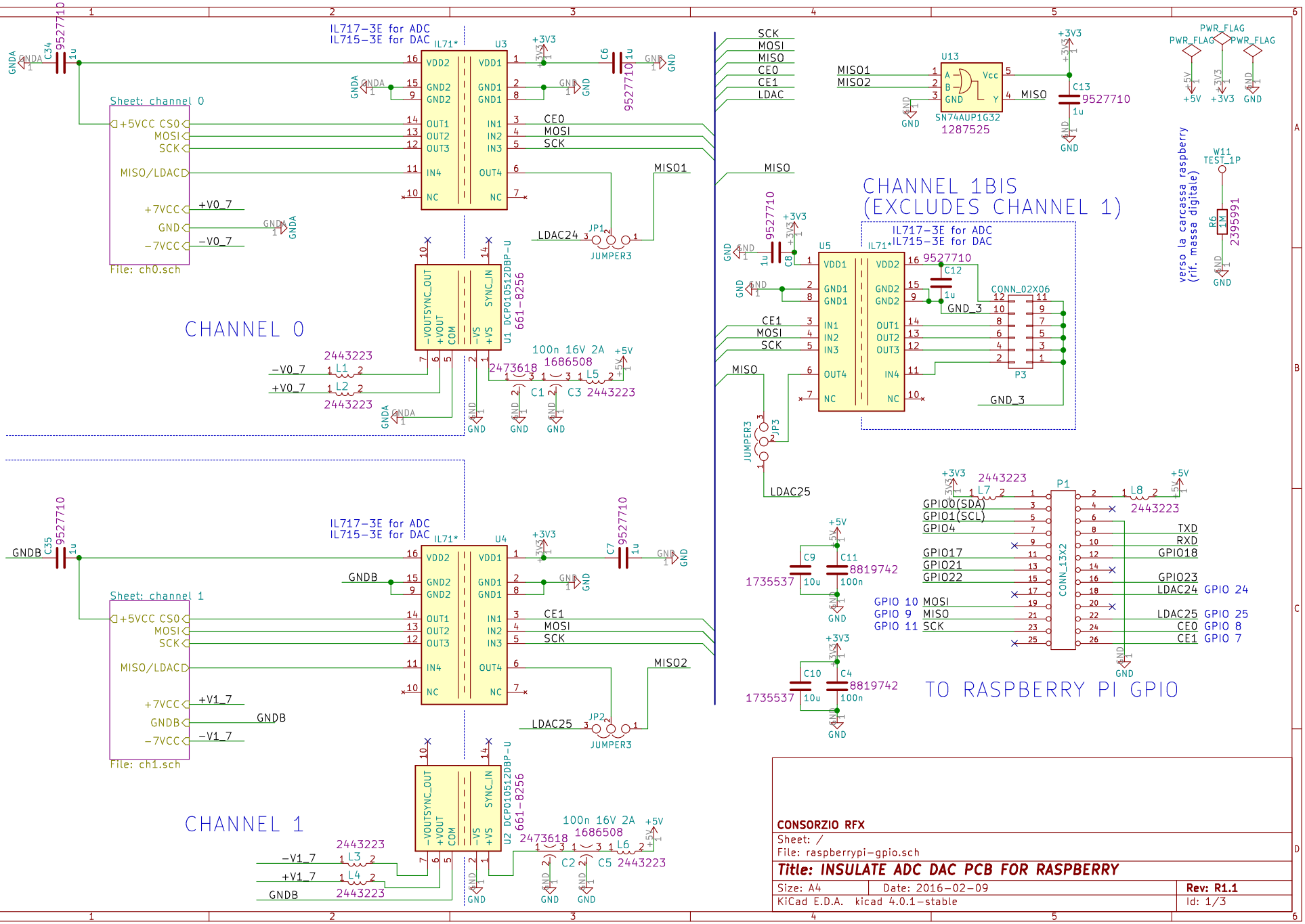

CONSORZIO RFX

Sheet: /
File: raspberrypi-gpio.sch

Title: INSULATE ADC DAC PCB FOR RASPBERRY

Size: A4	Date: 2016-02-09	**Rev: R1.1**
KiCad E.D.A. kicad 4.0.1-stable		Id: 1/3

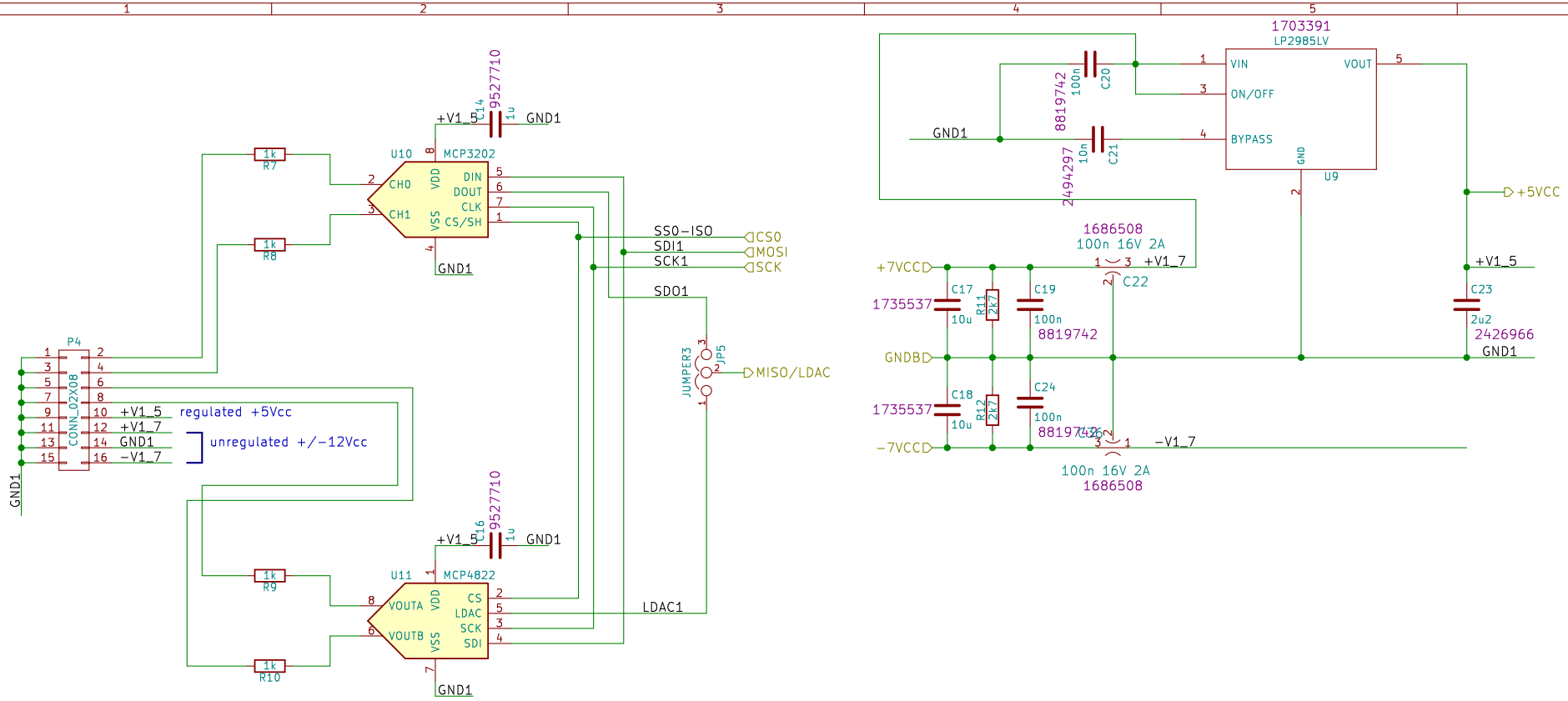

USE ONLY ONE DIGITALIZER

CONSORZIO RFX		
Sheet: /channel 1/		
File: ch1.sch		
Title: INSULATE ADC DAC PCB FOR RASPBERRY		
Size: A4	Date: 2016-02-09	**Rev: R1.1**
KiCad E.D.A. kicad 4.0.1-stable		Id: 2/3

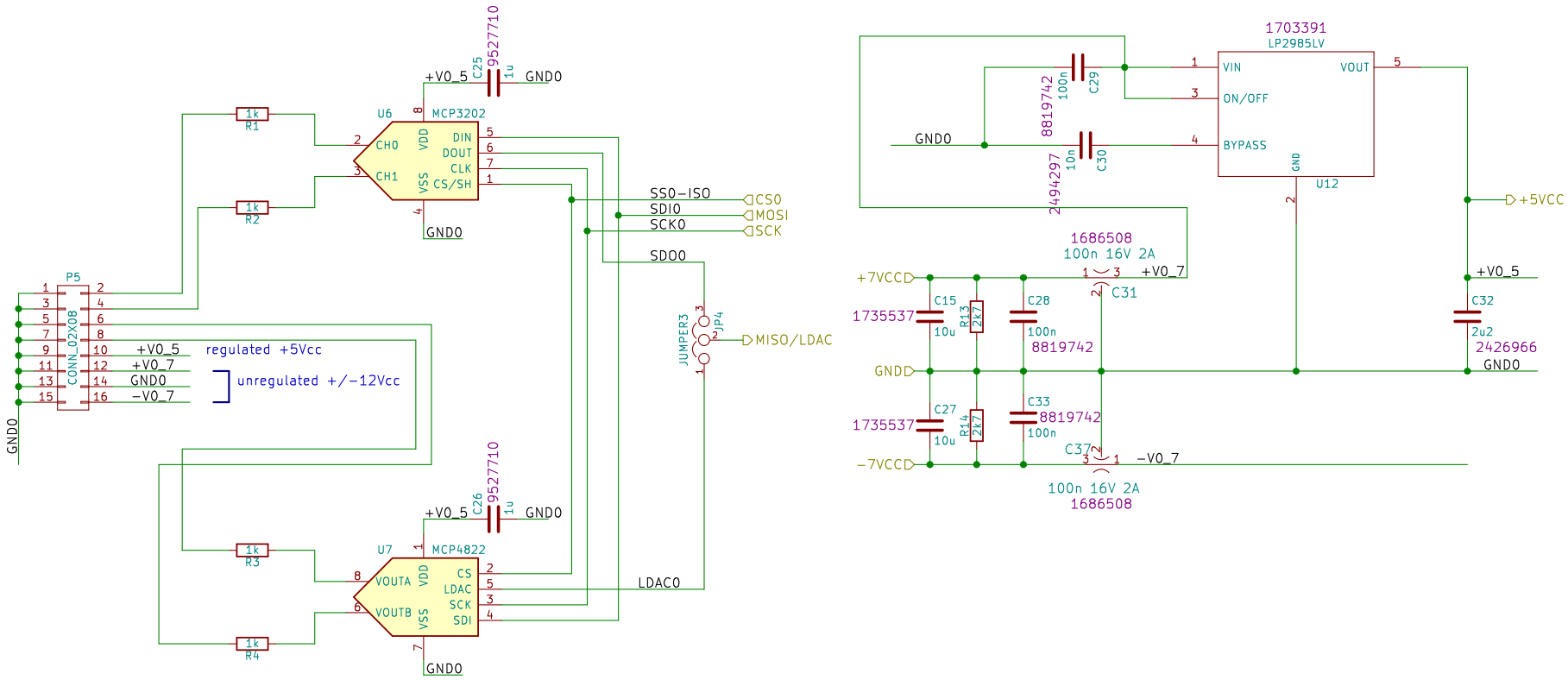

USE ONLY ONE DIGITALIZER

CONSORZIO RFX		
Sheet: /channel 0/		
File: ch0.sch		
Title: INSULATE ADC DAC PCB FOR RASPBERRY		
Size: A4	Date: 2016-02-09	**Rev: R1.1**
KiCad E.D.A. kicad 4.0.1-stable		Id: 3/3

4.2 SPI communication

Serial Peripheral Interface (SPI) is a synchronous serial data protocol used by microcontrollers for communicating with one or more peripheral devices quickly over short distances.

With an SPI connection there is always one controller device (also called master) which controls the peripheral devices (also called slaves).

Device communication primarily relies on four distinct lines:

- MISO (Master In Slave Out): which represents the peripheral line for sending data to the controller;
- MOSI (Master Out Slave In): which represents the controller line for sending data to the peripherals;
- SCK (Serial Clock): The clock signal used to synchronize data transmission;
- CS /SS (Chip Select): used to select the device when multiple peripherals are used on the same SPI bus

In our case, the SPI connection is used to allow the controller ESP32 to communicate with the ADC and DAC by using a common SPI bus (called VSPI) as depicted in Fig.38.

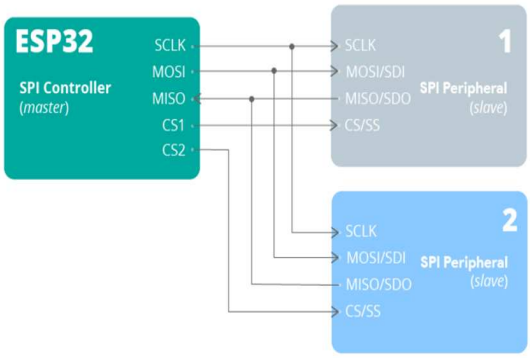

Figure 38: SPI communication scheme.

Communication with the MCP3202 is done using a standard SPI-compatible serial interface. In most microcontroller SPI ports, data is transmitted in

groups of eight bits. Additionally, the SPI port configuration typically involves data being clocked out on the falling edge of the clock signal and latched in on the rising edge. To ensure reliable communication and avoid issues, the microcontroller may need to send extra clock pulses. This is usually done by sending 'leading zeros' before the start bit (which are ignored by the device) as depicted in Fig.39.

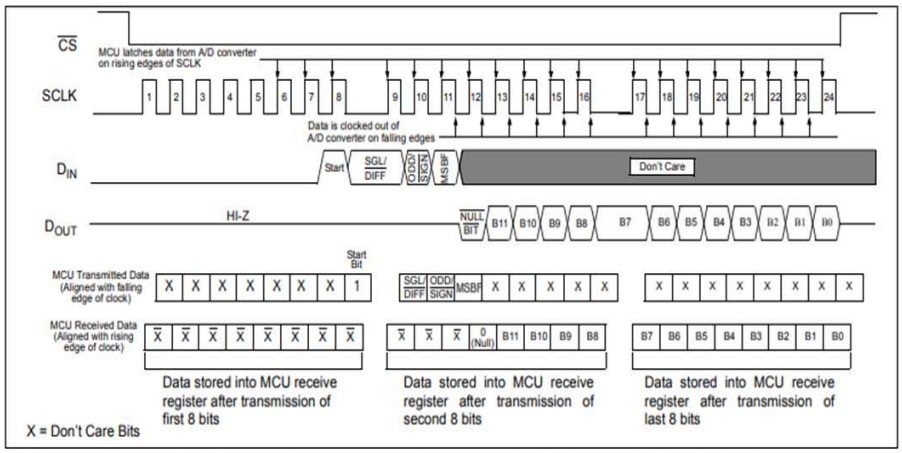

Figure 39: SPI Communication using 8-bit segments (Mode 0,0: SCLK idles low).

It is therefore necessary to increase the number of clock pulses to prevent communication errors between the ESP32 and the MCP3202. This, along with the need to process the three groups of 8 bits containing the sampled data, results in a reduction of the maximum sampling frequency to 53 ksps. Despite this reduction, the sampling frequency is significantly higher than the limit sampling frequency set by the Nyquist–Shannon theorem.

4.3 Asynchronous demodulation

The computational time necessary for processing the sampled data and calculate a coherent output signal for the MCP4822 leads to a further increase of the sampling time. As depicted in Fig.40, the sampled pickup voltage characteristic obtained with a synchronous demodulation technique, appears to be too coarse to obtain precise value to work with.

The problem is overcome by using an asynchronous demodulation approach. The Arduino code is structured in order to ask the ADC to acquire N number of readings, before closing the communication with it. After that, the code proceed to process the data and compute the output signal for the DAC.

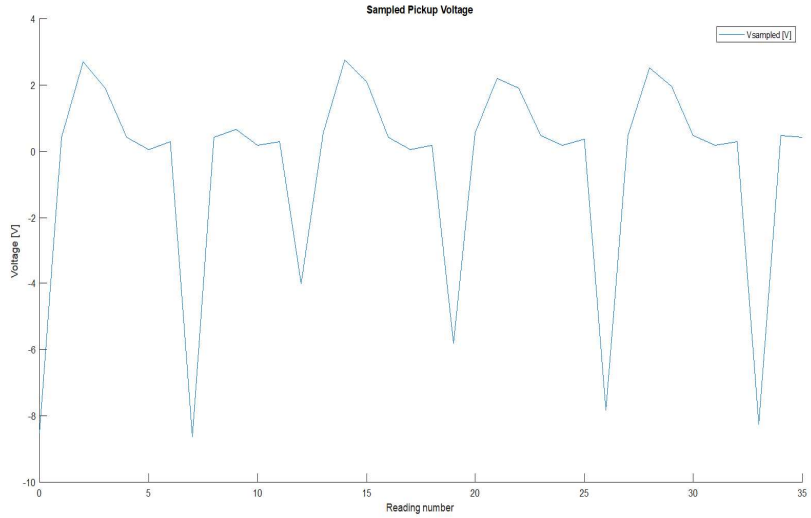

Figure 40: Plot of the sampled pickup voltage.

By using this approach:

- The digital low-pass filter is used to attenuate noises at a frequency higher than 1 kHz. This allows to obtain a smoother characteristic of V_{sense} as depicted in Fig.41

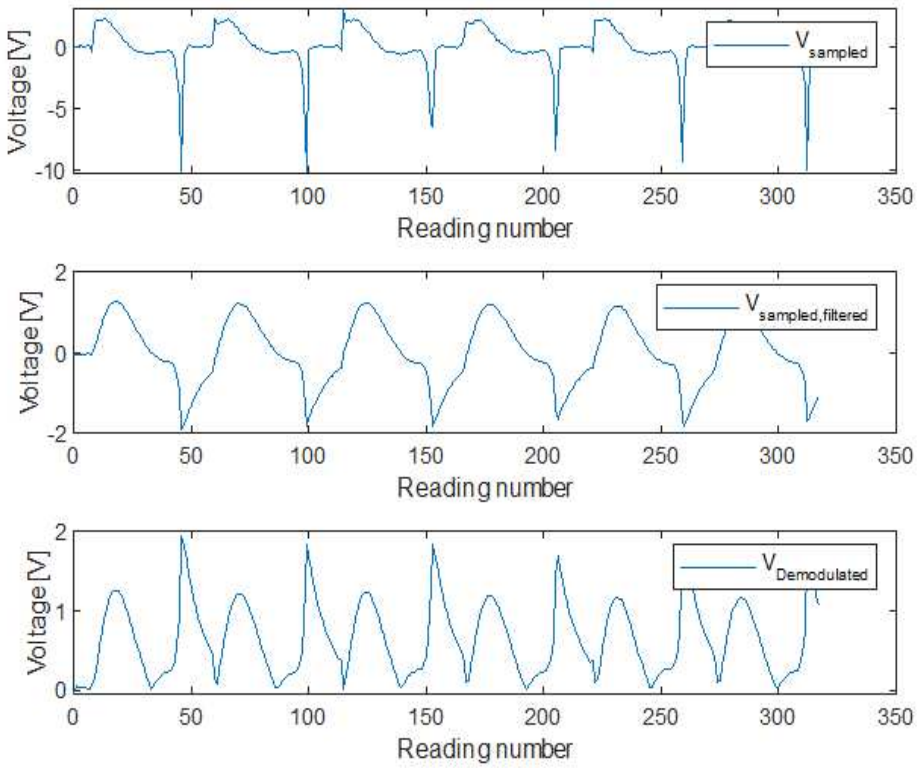

Figure 41: Plots showing sampled pickup voltage, filtered sampled pickup voltage, and demodulated voltage characteristic.

- The error is calculated by performing the arithmetic mean of the demodulated voltage characteristic defined by the eq.11. Thus, the filter is no longer used to calculate the DC value.

4.4 System calibration

System calibration reduces noise errors associated to the sensor system and the reading instrumentation, allowing a more precise data processing. The different readings of the pickup voltage, acquired for different values of beam current, was used to:

- Determinate the offset error associated to the V_{sense} characteristic at zero value of beam current. This offset, calculated over one thousand readings, allowed to perform better calculations of the error associated to intensity values of I_{beam} close to zero.
- Determinate the average error at different values of I_{beam}. This step permitted:
  - The definition of the reference set point to be used in the digital PID. The reference value is calculated by averaging the mean error calculated for different set of readings at zero beam current.
  - The assessment of the linear relationship linking beam current intensity to the computed average error. The results of the linearity assessment are reported in Fig.42

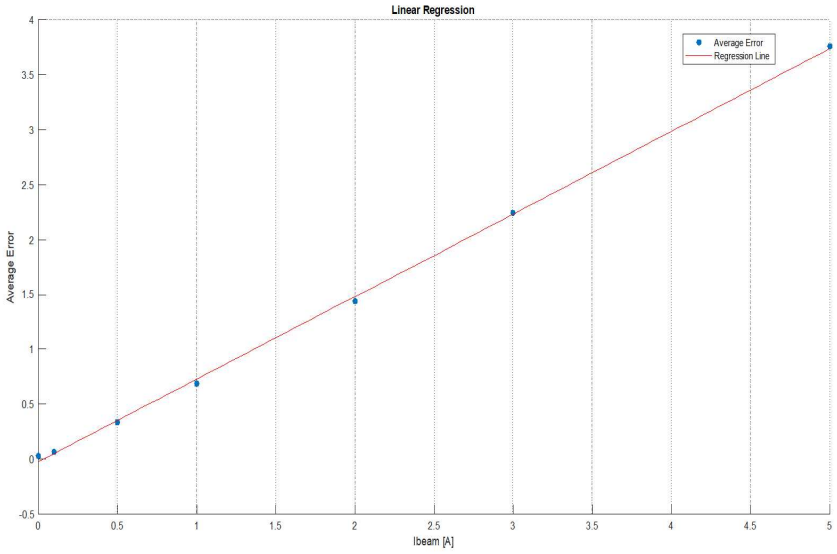

Figure 42: Illustration of the linear relationship between I_{beam} and the average error calculated from the sampled data.

The error calculated using eq.11 is always positive, which means that the information of the sense of I_{beam} is lost during the demodulation process of the signal. A beam current of 1 A or -1 A inevitably leads to the same error.

It is therefore necessary to define an unit vector which is used to direct the digital PID controller to the right direction. This problem is assessed by using the pick-to-pick difference of the pickup voltage. Fig.43 shows that the difference changes its sign depending on the sense of I_{beam}

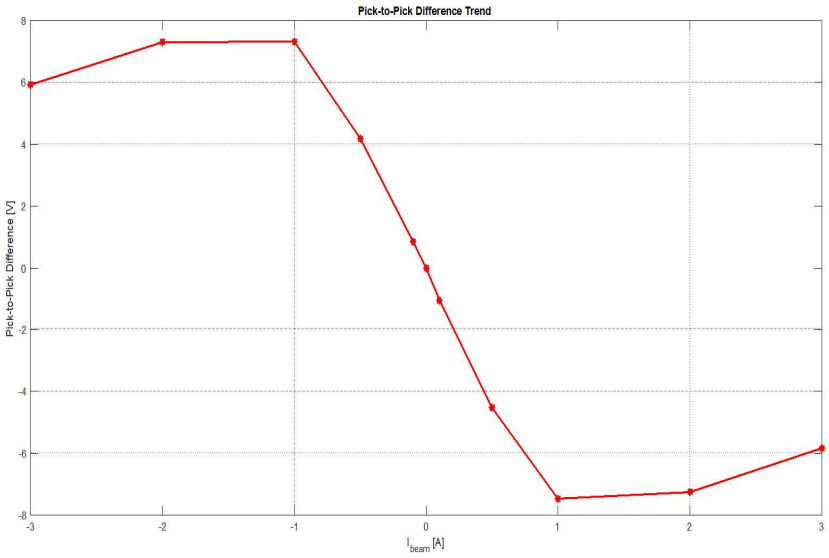

Figure 43: Pick-to-pick trend as a fuction of I_{beam}

5 Results

After the system calibration, the communication with the DAC was enabled, allowing the generation of a controlled output voltage (V_{DAC}) used to drive the compensation current generator. The system response at different values of I_{beam} is reported in Fig.44 .

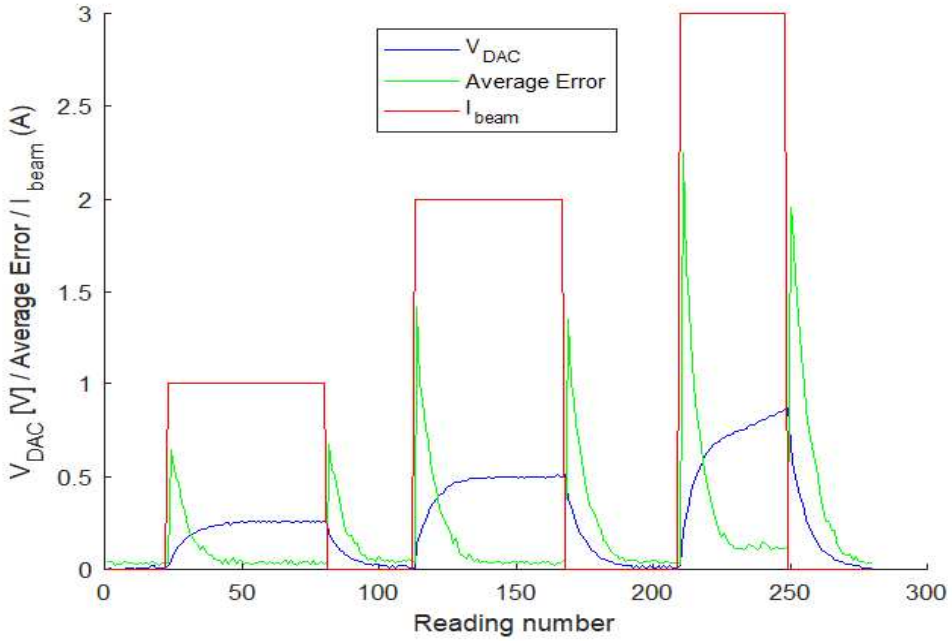

Figure 44: V_{DAC} and Average Error response as a function of I_{beam}.

The results obtained follow a desired trend. The error generated by a current step is proportional to the intensity of Ibeam and is appropriately processed by the PID to generate an output voltage on the DAC. In this way, the compensation current begins to flow into the feedback circuit, reducing the error until the steady-state conditions are reached. When I_{beam} is set to zero, the unit vector opportunely change the sign of the error, bringing the compensation current to zero. As depicted in Fig.44, a value of I_{beam} of 3 A, exceed the compensation capability of the prototype. This limitation can be addressed by increasing the number of turns of the compensation winding.

6 Conclusion

The numerical and physical realization of a DCCT sensor prototype has allowed for a deeper understanding of its control electronics. The results obtained and the implemented setup reveal numerous areas for improvement, especially in view of electronics implemented via FPGA.

It is possible to investigate the performance of the system by implementing a synchronous control. This involves utilizing two separate CS channels (VSPI and HSPI) for the ADC and DAC (Fig.45). In this way, it is possible to implement the dual-core function of the ESP32 microcontroller: one core can focus on reading sensor output, while the other manages data processing and DAC communication. This approach enables a more responsive control system.

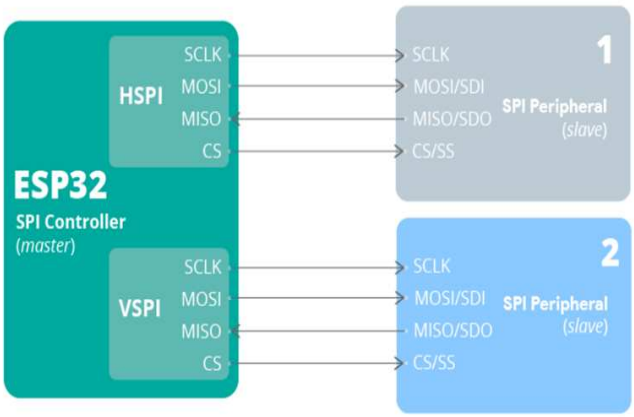

Figure 45: Dual core SPI communication scheme

7 Acknowledgements

I want to express my gratitude to my family for their support and encouragement throughout my academic journey. A special thanks to Prof. Eng. Marconato Nicolò and Eng. Laterza Bruno, whose valuable contribution and guidance enriched my research work.

Heartfelt thanks to Sonia, who supports me with love and patience in every aspect. Also, thanks to friends with whom I've shared many adventures.

References

[1] RFX; URL: https://www.igi.cnr.it/

[2] Rev. Sci. Instrum. 90, 033303 (2019);
URL: https://doi.org/10.1063/1.5087804

[3] Soliman, E., et al. Sensor Studies for DC Current Transformer Application.

[4] Forslund, Åke. "Designing a Miniaturized Fluxgate Magnetometer." Master's thesis, Stockholm University, 2006

[5] Magnetic Sensors and magnetometers
(P. Ripka et al) ISBN: 1580530575

[6] Magnes, W., Pierce, D., Valavanoglou, A., Means, J., Baumjohann, W., Russell, C. T., Schwingenschuh, K., & Graber, G. (2003). A sigma–delta fluxgate magnetometer for space applications. Measurement Science and Technology, 14(7), 1003.
URL: https://dx.doi.org/10.1088/0957-0233/14/7/314

[7] Liu SW, Liu SB. Design and Realization of a Digital Multichannel Fluxgate Signal Processing System. AMM 2012;182–183:491–5. https://doi.org/10.4028/www.scientific.net/amm.182-183.491.

[8] Dr.Steve Arar, Synchronous demodulation;
URL: https://www.allaboutcircuits.com/author/dr-steve-arar

[9] PSIM user manual;
URL: https://powersimtech.com/wp-content/uploads/2021/01/PSIM-User-Manual.pdf

[10] Microchip Technology, MCP3202
URL: https://www.microchip.com/en-us/product/mcp3202

[11] Arduino Docs
URL: https://docs.arduino.cc/